Neuron, Volume *72*

Supplemental Information

Recurrent Circuitry Dynamically Shapes the Activation of Piriform Cortex

Kevin M. Franks, Marco J. Russo, Dara L. Sosulski, Abigail A. Mulligan, Steven A. Siegelbaum, and Richard Axel1

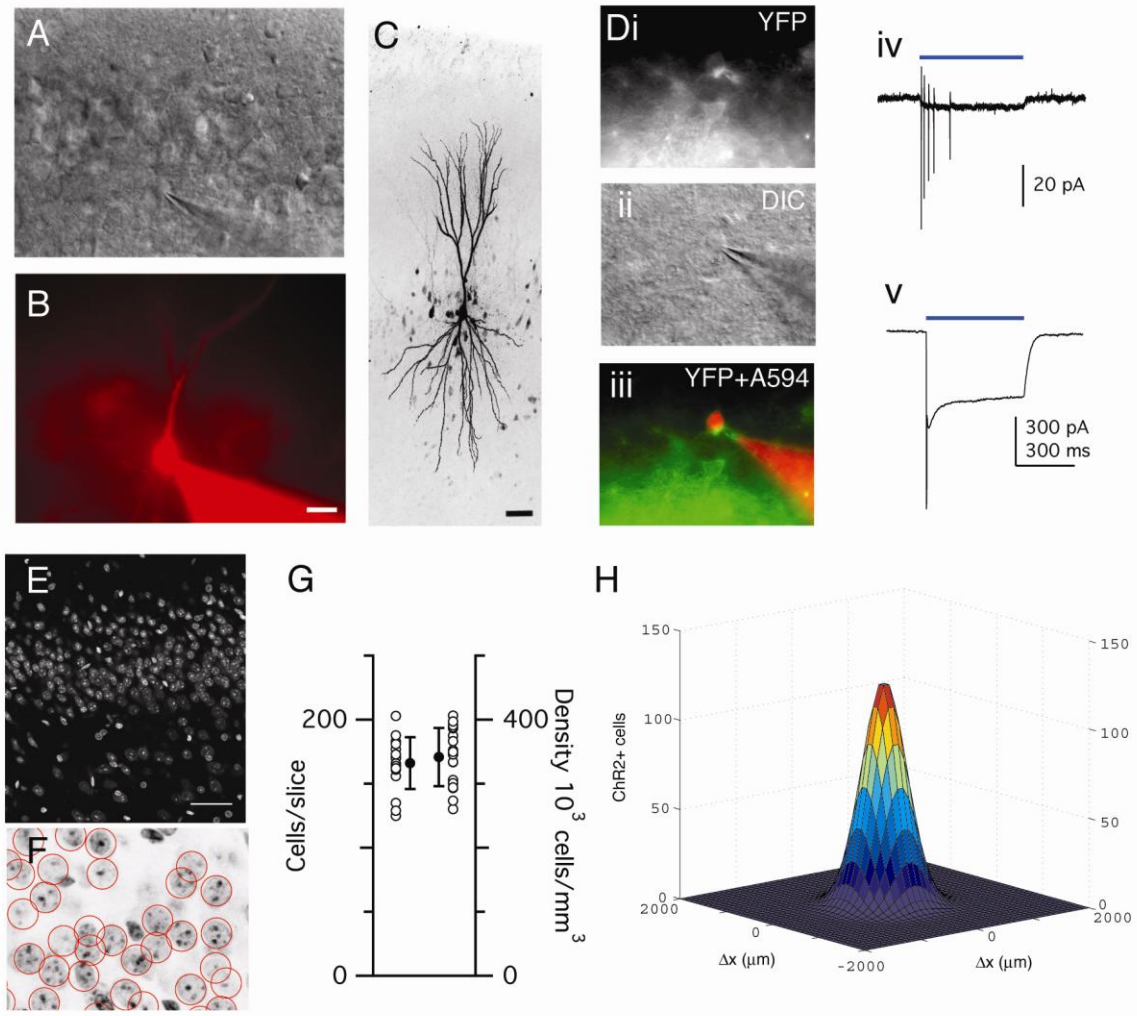

Supplemental Figure 1

Figure S1 (related to Figure 1). **Channelrhodopsin expression in a subset of piriform cortex neurons**

Cells in piriform cortex were visualized with DIC optics (A) and recorded with Alexa594-cadaverine (B) in the intracellular solution to confirm that we were recording from deep layer II pyramidal cells. Scale bar, 10 μm. (C) After recording, slices were fixed and stained to reveal biocytin label for post hoc confirmation that all recorded cells were layer II pyramidal cells. Scale bar, 20 μm. (D) YFP-expressing cells were $ChR2^+$. (i) FITC and (ii) DIC images showing a targeted recording from a YFP-expressing cell at the edge of the fluorescence cloud. (iii) Shows merged images with Alexa594 in the intracellular solution; scale as in C. Weak (25 mW) light pulses evoked spiking, as seen in cell-attached recordings (iv) and inward currents in whole-cell recordings (v) from this cell. (E) Nissl-stained section of anterior piriform cortex (scale bar, 50 μm). (F) Inverted, contrast-enhanced area from E used to count individual layer II nuclei (red circles). (G) Number of counted cells (mean ± S.D., 166 ± 20) and extrapolated density of cells ($342 \pm 45 \cdot 10^3$ cells/mm^3; 18 sections from 2 animals). (H) Distribution of $ChR2^+$ excitatory neurons estimated from the total density of layer II neurons and the probability of patching a $ChR2^+$ cell at a given distance from the injection center. Each block corresponds to a 0.1 mm x 0.1 mm x 0.1 mm column in layer II.

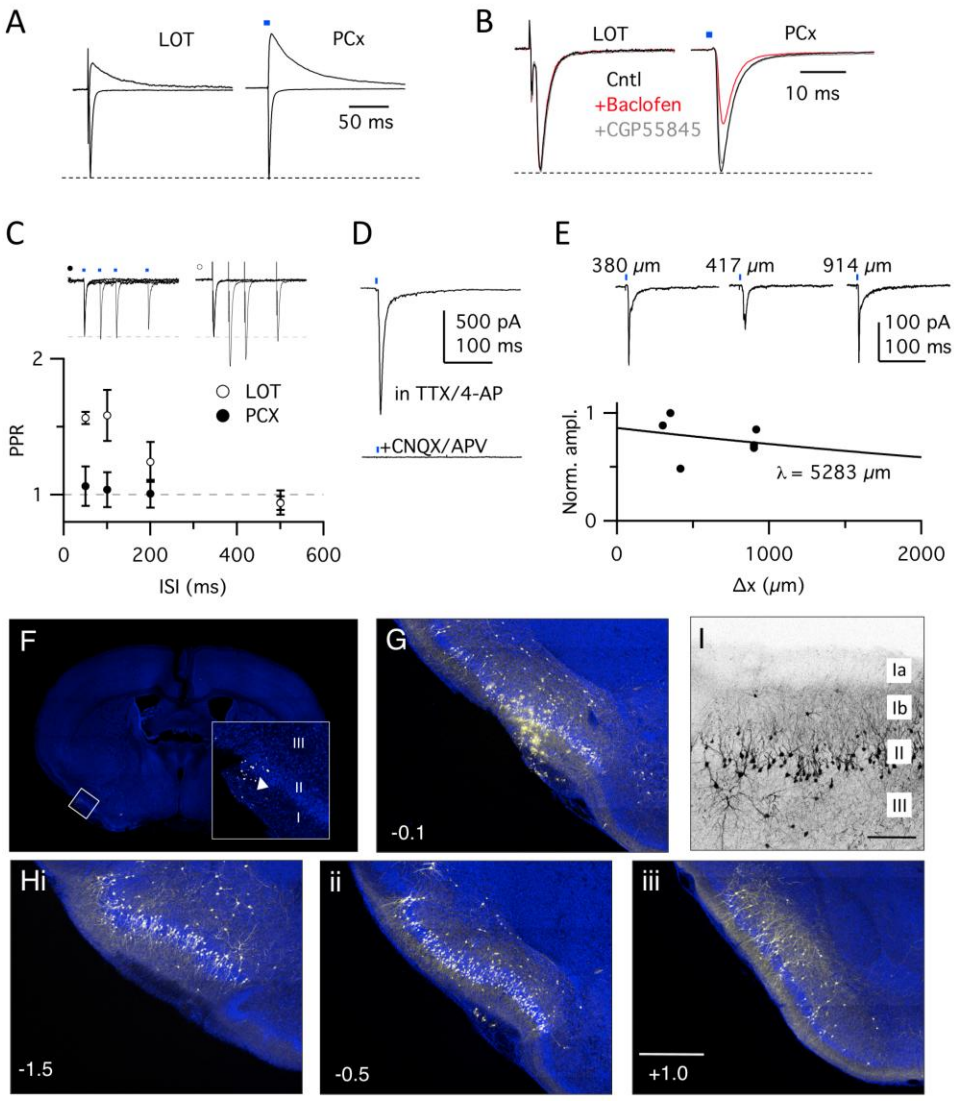

Supplemental Figure 2

Figure S2 (related to Figure 2) **Monosynaptic "associational" synaptic responses evoked by light in layer II pyramidal cells**

The synaptic properties of light-evoked responses in layer II pyramidal cells following ChR2 expression in piriform cortex were consistent with those described for "associational" piriform synapses. (A) An example of voltage-clamp recordings at -70 mV and +50 mV in GBZ following LOT stimulation (left) and light pulses (right). In the same cells, recurrent synapses have significantly greater responses at +50 mV than afferent synapses, consistent with the high levels of NMDA receptors expressed at these synapses. Responses are normalized to the response at -70 mV. (B) Light-evoked synaptic responses were suppressed in the $GABA_B$ agonist baclofen and rescued by subsequent administration of the $GABA_B$ antagonist CGP55845. LOT-evoked responses in the same cells were insensitive to baclofen or GGP55845. (C) Paired pulses facilitated EPSCs evoked by electrical stimulation of the LOT but had no net effect on light-evoked responses in the same cells. (D) Large light-evoked EPSCs recorded in a cell far from the infection site ($\Delta x > 800$ μm) in the presence of TTX, 4-AP and GBZ. These responses were blocked by CNQX and D-APV. (E) Light-evoked EPSCs recorded at different Δx showed minimal decrement with distance from the infection site in the presence of TTX/4-AP. Note, the responses shown here are somewhat smaller than usual as they were evoked by focal illumination of layer Ib rather than wide-field illumination. Together, the large amplitude of these responses and their invariance with respect to distance from the infection site in the presence of TTX indicate that the large light-evoked responses observed under control conditions are monosynaptic inputs that originate from $ChR2^+$ axons that project across the extent of piriform, rather than from a wave of polysynaptic excitation that cascades across piriform cortex. (F) A modified, GFP-expressing rabies virus that can efficiently infect presynaptic terminals, but

cannot spread beyond the infected cells, was focally injected into layer Ib/II. Inset shows fluorescent beads that were co-injected with rabies virus to verify the location of the injection site. Labeling of pyramidal cells was observed at the site of injection (G) and across the piriform (H). Numbers in the bottom left corner of the panels indicate distance from the injection site, in mm. Scale bar, 1 mm (I) Magnified and contrast-enhanced image of GFP signal from Hii. Scale bar, 100 μm. The frequency of infected cells was only minimally dependent upon the distance from the injection site, particularly in the rostral direction (in mm). A greater fraction of layer III pyramidal cells were labeled in more caudal sections, consistent with the observation that these cells project from posterior to anterior piriform cortex. (Datiche et al., 1996; Haberly and Price, 1978). Scale bar, 500 μm.

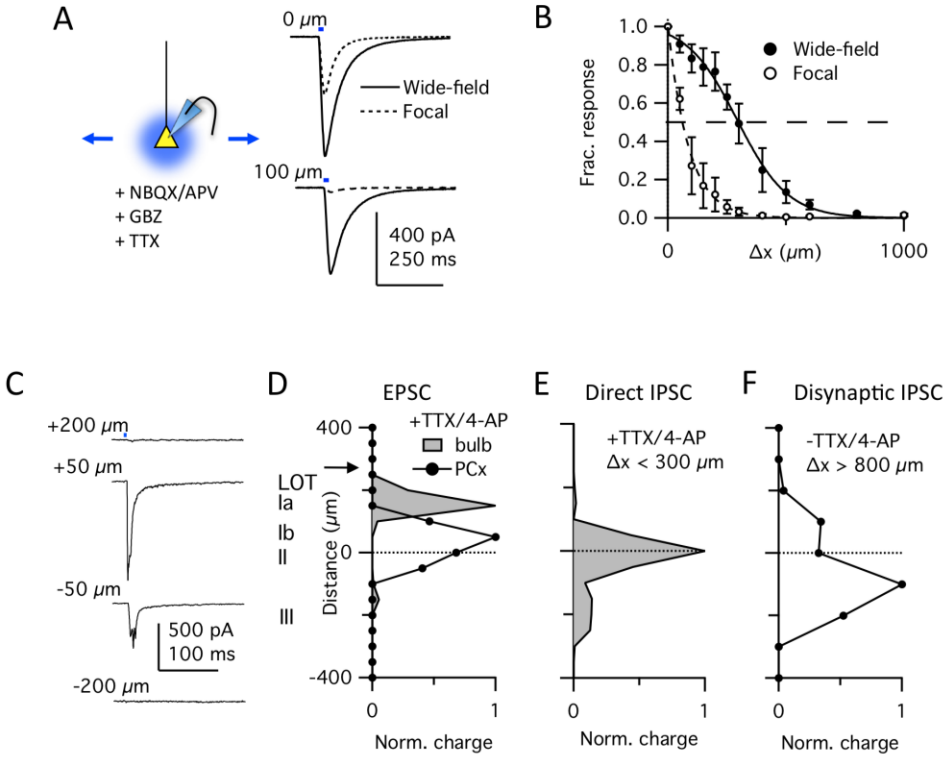

Supplemental Figure 3

Figure S3 (related to Figure 3) **Focal illumination indicates laminar organization of excitatory and inhibitory inputs**

(A) Strategy for determining size of excitation field. Photocurrents were isolated by recording from $ChR2^+$ cells in the presence of NBQX, APV, GBZ and TTX. The amplitude of the isolated photocurrent was measured following light pulses presented at different distances from the cell body along layer II, normal to the apical basal axis of the cell. Full-field and focal light pulses were evoked when an aperture in the light path was either open (solid line) or closed (dashed line), respectively. (B) Normalized photocurrent amplitudes as a function of light distance from the soma with the aperture open (filled circle, n=5) or closed (open circle, n=5). The size of full-field response was described by a Gaussian distribution (width, 370 μm). The size of the focal phorocurrent was fit with a single exponential, (87 μm). (C) EPSCs evoked by focal illumination along the apical-basal axis of a cell in TTX, 4-AP and GBZ to restrict transmitter release to the field of illumination and determine the dendritic locus of $ChR2^+$ synapses (soma = 0 μm, positive distances in apical direction). (D) Excitatory synaptic responses (normalized charge) plotted on x-axis as a function of light spot location along the cell's apical-basal axis (y-axis). Locations of different layers are indicated to the left of the ordinate. Arrow indicates average location of pial surface. EPSCs were measured following viral expression of ChR2 in either piriform cortex (black line) or mitral/tufted cells in the olfactory bulb (gray shading). (E) Site of synaptic inputs from $ChR2^+$ interneurons was determined by recording inhibitory responses (+5 mV) along the apical-basal axis of cells close to the center of infection ($\Delta x < 400$ μm) in TTX, 4-AP, NBQX and APV. (F) Locus of excitatory $ChR2^+$ inputs onto feedback interneurons was determined by recording inhibitory responses from layer II pyramidal cells far

from the infection focus ($\Delta x > 800$ μm) in the absence of any receptor antagonists or channel blockers.

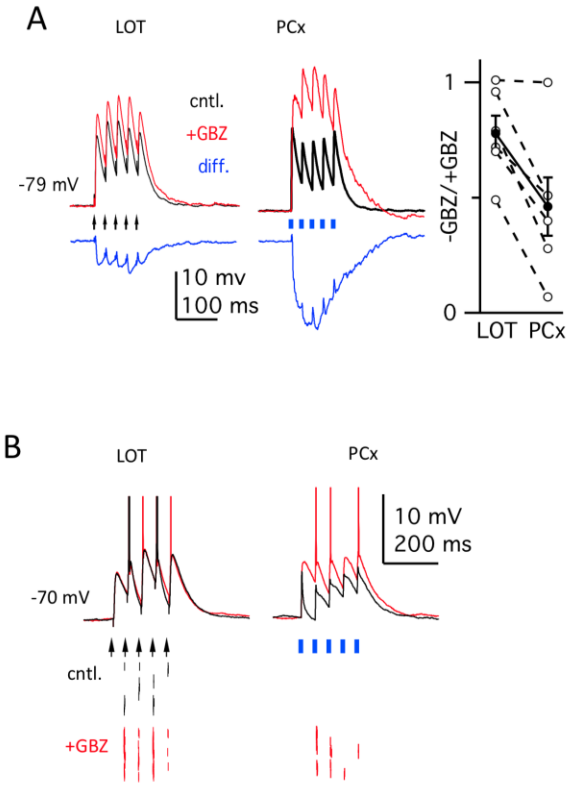

Supplemental Figure 4

Figure S4 (related to Figure 4). **Strong feedback from recurrent activation controls pyramidal cell spiking**

(A) Left: EPSPs evoked by LOT stimulation or light pulses before (black traces) and after (red traces) GBZ application in pyramidal cells distant from the site of infection ($\Delta x > 800$ μm). The difference between the two responses, which reveals the GABAergic suppression, is shown in blue. Right: Ratio of the integrated EPSPs (300 ms) with and without GBZ in response to LOT and PCx stimulation. Feedforward inhibition decreased the size of the LOT-evoked EPSP by 20% (0.79 ±0.092; n=5 cells; paired t-test, p=0.091; Figure 4E), indicating a relatively small role for feedforward inhibition in suppressing piriform pyramidal cells. In contrast, feedback inhibition decreased the size of the recurrent EPSP by 50% in the same cells (0.47 ± 0.15; paired t-test, p=0.027), indicating its more prominent role in inhibiting piriform. Open circles represent data from individual cells; filled circles are the average across cells, showing greater suppression by feedback inhibition elicited by PCx stimulation (n=5; p = 0.026). (B) Recordings showing response to same LOT and PCx stimuli before and after blocking inhibition with GBZ. Responses were compared at the lowest stimulus intensity that reliably drove spiking when inhibition was blocked. Bottom: spike raster plots.

Supplemental Experimental Procedures

All experiments used C57BL/6 mice from Jackson Laboratories and followed approved national and institutional guidelines of the Columbia University Medical Center.

Virus production and injections

Cre Recombinase-GFP (Le et al., 1999) was cloned into a lentivirus vector behind a human Synapsin promoter. High-titer lentivirus was either prepared using established protocols (Zhang et al., 2010) or produced commercially (System Biosciences, 8.55 x 10^8 IFU/ml). Adeno-associated virus was generated from a pAAV-EF1a-DIO-hChR2(H134R)-EYFP-WPRE-pA plasmid (gift from Karl Deisseroth) and produced commercially (UNC Vector; serotype 2/1; 4 x 10^{12} IFU/ml). Viruses were separated into 4 μL aliquots and stored at -80^{o}C.

Young adult C57/BL6 mice (4-8 weeks old) were anaesthetized with ketamine/xylazine (100/10 mg/kg, respectively, ip) and head-fixed in a stereotaxic device. Virus was injected with a pulled glass pipette using standard procedures (Cetin et al., 2006). Briefly, an incision was made in the scalp and a small craniotomy was drilled above the anterior piriform cortex using sterotaxic coordinates optimized by fluorescent bead injection (FluoSpheres, Invitrogen). Individual aliquots of lentivirus and AAV were thawed, mixed (1:1), and slowly pressure injected through a glass pipette (tip size, ~20 μm; 681 ± 64 nl, range 200-1250 nl). The pipette was left in place for 5 minutes before being slowly retracted. The same procedure was used for injections into somatosensory cortex, visual cortex and olfactory bulb, except that AAV2/5-Syn-hChR2(H134R)-EYFP (produced from the plasmid pAAV2/5-Syn-hChR2(H134R)-EYFP-WPRE-pA, gift from Karl Deisseroth) was injected into olfactory bulb. Off-target injections

resulted in no expression or expression that was largely absent from piriform cortex, and argue against spurious activation from other brain regions that were sometimes infected following virus injection. Animals with off-target infection were not used.

Rabies virus (SAD-ΔG-EGFP, gift from Ed Callaway) was amplified as described (Wickersham et al., 2007). Anesthetized mice were head fixed with a metal post cemented to the skull, and a small hole was drilled on the ventrolateral surface of the skull after retracting the overlying musculature. Rabies virus (~200 nL) and fluorescent beads were coinjected into layer Ib/II of piriform cortex. After 5 days, the animals were killed and processed histologically, as described below.

Electrophysiology and Analysis

Eighteen ± 1 days (range 13-28) after virus injection, mice were anesthetized with isofluorane and decapitated. The cortex was quickly removed in ice-cold artificial CSF (aCSF). Parasagittal brain slices (300 μm) were cut using a vibrating microtome (Leica) in a solution containing (in mM): 10 NaCl, 2.5 KCl, 0.5 $CaCl_2$, 7 $MgSO_4$, 1.25 NaH_2PO_4, 25 $NaHCO_3$, 10 glucose, and 195 sucrose, equilibrated with 95% O_2 and 5% CO_2. Slices were incubated at 34°C for 30 min in aCSF containing: 125 mM NaCl, 2.5 mM KCl, 1.25 mM NaH_2PO_4, 25 mM $NaHCO_3$, 25 mM glucose, 2 mM $CaCl_2$, 1 mM $MgCl_2$, 2 NaPyruvate. Slices were then maintained at room temperature until they were transferred to a recording chamber on an upright microscope (Olympus Optical) equipped with a 40x objective (LUMPLFLN 40XW, 0.8 N.A.). Patch electrodes (3-6 MΩ) contained: 130 D-Gluconic acid, 130 CsOH, 5 mM NaCl, 10 HEPES, 12 phosphocreatine, 3 MgATP, 0.2 NaGTP, 10 EGTA, 0.05 AlexaFluor 594 cadaverine, 0.15% biocytin. For current clamp recordings, electrodes contained: 130 Kmethylsulfnoate, 5 mM

NaCl, 10 HEPES, 12 phosphocreatine, 3 MgATP, 0.2 NaGTP, 0.1 EGTA, 0.05 AlexaFluor 594 cadaverine, 0.15% biocytin. Voltage- and current-clamp responses were recorded with a Multiclamp 700A amplifier, filtered at 2-4 kHz, and digitized at 10 kHz (Instrutech). Series resistance was typically ~10 MΩ, always <20 MΩ, and was compensated at 80%–95%. The bridge was balanced using the automated Multiclamp function in current clamp recordings. Data were collected and analyzed off-line using AxographX and IGOR Pro (Wavemetrics).

Short, collimated light pulses from a 470 nm LED (LEDC5, Thor Labs; 0-250 mW measured at the sample) were delivered to the tissue through the objective every 10-15 seconds. In most experiments we used a 2 ms, 250 mW pulse. In some experiments, a field-stop aperture in the light path was closed restricting illumination to a focal point (see below).

In a subset of experiments, we noted Δx for each recorded cell (166 cells from 11 slices/11 animals). We first determined whether these cells were $ChR2^+$ or $ChR2^-$, and whether $ChR2^-$ cells exhibited light-evoked EPSCs at -70 mV (n=96) or IPSCs at +5 mV (n=87). Addiotionally, some cells (n=71) were recorded at +5 mV in the presence of NBQX/APV to test for direct IPSCs. The cells from all experiments were pooled and binned with respect to Δx (200 μm bins), from which the observed probabilities (Figures 1E, 1G and 3B) were determined. NBQX or CNQX (10 μM), D-APV (50 μM), gabazine (i.e. SR95531 (10 μM), TTX (1 μM) and 4-AP (100 μM) were all obtained from Tocris. We did not correct for liquid junction potentials. All experiments were done at 34°C. Traces typically represent averages of 6-10 trials. Unless stated otherwise, data are presented as mean ± s.e.m.

Identification of layer II pyramidal cells

Neurons were patched in deep layer II under DIC optics and visualized at 590 nm with a monochrometer and cooled CCD camera (TiLL Photonics). Pyramidal cells were identified based on morphological and electrophysiological indicators (Haberly, 2005; Suzuki & Bekkers, 2009), including one or two spiny apical dendrites that branched extensively and extended to layer Ia and basal dendrites that extended into layer III, and input resistances of 100-200 MΩ (124 ± 8.4 MΩ). Recordings from semilunar cells or high input resistance layer II GABAergic neurons could readily be distinguished from pyramidal cells and were discontinued. After recording, slices were fixed and processed to visualize the biocytin label, confirming that patched cells were layer II pyramidal cells (Figure S1).

Photoillumination field

We measured the size of the illumination field by recording from $ChR2^+$ neurons in TTX, NBQX, D-APV and GBZ to isolate photocurrents. Light pulses were presented at different distances from the cell, normal to the apical-basal axis of the dendrites (Figure S3A). Light pulses were presented when an aperture in the LED light path was either open or closed, for wide-field illumination or focal illumination, respectively. The relationship between the photocurrent amplitude and distance from the recorded cell evoked with wide-field illumination was well fit by a Gaussian (width, 368 μm). The distance-dependence following focal illumination was fit with a single exponential function with a length constant of 87 μm (Figure 3B).

Synapse mapping

For localizing synaptic inputs, responses were recorded in TTX to block action potentials and 4-AP to enhance photoactivation of $ChR2^+$ synaptic terminals. The light spot was first centered on the soma and light pulses were then presented at 50 μm steps along a straight line extending from 400 μm apical to the soma to 400 μm basal to the soma. The pial surface was 308 ± 23 μm (n=10) apical to the soma. Responses evoked at each location (6-10) were averaged and normalized to the maximal average response recorded in that cell. Normalized response profiles from all cells were averaged and deconvolved in MatLab using the Lucy-Richardson algorithm with PSF=87 μm. For localizing excitatory and inhibitory synaptic inputs, responses were recorded in GBZ or NBQX and D-APV, respectively. For localizing the origin of disynaptic inhibition, the same procedure was used except that responses were evoked with no drugs present and with $\Delta x > 1{,}000$ μm. Slices were placed in the recording chamber with the pial surface/LOT at the top of the chamber and apical-basal axis of layer II pyramidal cells was roughly aligned along the vertical axis. Misalignment of this axis, lateral spread of dendrites and dendritic filtering all bias the efficacy of somatic measurements, and were not corrected.

Estimation of total number of $ChR2^+$cells

Variability in the number of $ChR2^+$ cells from animal to animal required that we determine the number of $ChR2^+$ cells from the same animals in which we performed quantitative electrophysiological experiments. We were not able to resolve individual $ChR2^+$ cells in the 300-μm slices used in electrophysiology experiments, or reliably resection these slices for posthoc analysis. We therefore estimated the average number of layer II $ChR2^+$ neurons per animal from the observed distribution of $ChR2^+$ cells with distance from the injection center and an estimate

of the total layer II cell density. Confocal images of Nissl-stained sections (NeuroTrace640; 1:500; 10 μm optical sections) were used to count the number of layer II nuclei in a region of anterior piriform cortex (Figure S1F, G). Only in-focus nuclei with well-defined boundaries were counted. Small, heterochromatic nuclei with intense label were not counted, as these were likely to be glia (Nauta and Feirtag, 1986). We counted 166 ± 20 layer II nuclei in delimited area of layer II of 0.044 ± 0.005 mm^2 (18 sections from two animals). We corrected for the estimated 10% of inhibitory layer II neurons (Loscher et al., 1998; Mugnaini and Oertel, 1985). The sample space for each count was simplified to a rectangular cuboid with sides 440 μm (width of each image) x 100 μm (height of layer II) x 10 μm (depth defined by optical section), in which we determined a volume density of layer II excitatory neurons of 342 ± 45 x 10^3 cells/mm^3 (Figure S1H).

The probability of patching a $ChR2^+$ cell with distance from the injection site follows a normal distribution, and so we assume that the probability density for ChR2-positivity within the sheet of layer II cells can be described by a two-dimensional Gaussian curve, given as:

$$p(x,y) = A \cdot \exp\left(\frac{(x)^2}{2\sigma^2} + \frac{(y)^2}{2\sigma^2}\right),$$

where A = 0.37 (fraction of $ChR2^+$ cells at injection center) and $\sigma^2 = 223$ (Figure S1I). The total number of $ChR2^+$ neurons was then determined by integrating this probability density function over the estimated number of neurons in a 2 mm x 2 mm x 0.1 mm sheet of cells, discretized into 1,600 columns (0.1 mm x 0.1 mm x 0.1 mm), with the injection site at the center of the sheet. We estimate that we express $ChR2^+$ in 7,889 excitatory layer II neurons.

Histology and imaging

Animals were anesthetized with ketamine/xylazine and perfused through the heart with cold PBS followed by 4% paraformaldehyde. Brains were removed and postfixed overnight. Tissue was embedded in a 5% gelatin block and 100 μm-thick coronal sections were cut on a vibrating microtome (Leica). Slices were permeabilized (0.3% PBS-T) and incubated at 4 °C overnight in chicken anti-GFP (Invitrogen, 1:1000) and rabbit anti-Cre (Novagen, 1:1000) antibodies. Slices were rinsed and then incubated in donkey Alexa-488 anti-chicken and Alexa-555 anti-rabbit antibodies (1:1000) and NeuroTrace 640 (1:500; all Invitrogen) at 4 °C for 2-4 hours. Rinsed slices were mounted with Vectashield and visualized with a Zeiss 710 confocal microscope. For visualizing patched neurons, slices were removed from the recording chamber after recording and placed in 4% PFA overnight. Slices were permeabilized (0.3% PBS-T) and incubated at for 24-72 hours at 4 °C in a rabbit anti-GFP antibody (Invitrogen, 1:1000) and Alexa-555 conjugated Streptavidin (Invitrogen, 1:200). Slices were rinsed and incubated in donkey Alexa-488 anti-rabbit antibody and NeuroTrace 640 (Invitrogen, 1:500) 4 °C overnight. Rinsed slices were mounted with Vectashield and visualized on an upright fluorescent microscope.

Supplemental References:

Cetin, A., Komai, S., Eliava, M., Seeburg, P.H., and Osten, P. (2006). Stereotaxic gene delivery in the rodent brain. Nature Protocols *1*, 3166-3173.

Datiche, F., Litaudon, P., and Cattarelli, M. (1996). Intrinsic association fiber system of the piriform cortex: a quantitative study based on a cholera toxin B subunit tracing in the rat. J Comp Neurol *376*, 265-277.

Haberly, L.B., and Price, J.L. (1978). Association and commissural fiber systems of olfactory cortex of rat. 1. Systems originating in piriform cortex and adjacent areas. Journal of Comparative Neurology *178*, 711-740.

Le, Y., Miller, J.L., and Sauer, B. (1999). GFPcre fusion vectors with enhanced expression. Anal Biochem *270*, 334-336.

Loscher, W., Lehmann, H., and Ebert, U. (1998). Differences in the distribution of GABA- and GAD-immunoreactive neurons in the anterior and posterior piriform cortex of rats. Brain Res *800*, 21-31.

Mugnaini, E., and Oertel, W.H. (1985). An atlas of the distribution of GABAergic neurons and terminals in the rat CNS as revealed by GAD immunohistochemistry. In GABA and Neuropeptides in the CNS, A. Bjorklund, and T. Hokfelt eds. (Amsterdam, Elsevier), pp. 436-612.

Nauta, W.J.H., and Feirtag, M. (1986). Fundamental Neuroanatomy (New York, W.H. Freeman).

Wickersham, I.R., Finke, S., Conzelmann, K.K., and Callaway, E.M. (2007). Retrograde neuronal tracing with a deletion-mutant rabies virus. Nat Methods *4*, 47-49.